JBC RESEARCH ARTICLE

Structural insights into the specific interaction between *Geobacillus stearothermophilus* tryptophanyl-tRNA synthetase and antimicrobial Chuangxinmycin

Received for publication, December 22, 2021, and in revised form, January 6, 2022 Published, Papers in Press, January 12, 2022,
https://doi.org/10.1016/j.jbc.2022.101580

Shuai Fan[1,‡], **Guangxin Lv**[1,‡], **Xiao Feng**[1], **Guangteng Wu**[2], **Yuanyuan Jin**[1], **Maocai Yan**[3,*], **and Zhaoyong Yang**[1,*]

From the [1]*Institute of Medicinal Biotechnology, Chinese Academy of Medical Sciences & Peking Union Medical College, Beijing, China;* [2]*Research and Development Department, ArNuXon Pharm-Sci Co, Ltd, Beijing, China;* [3]*School of Pharmacy, Jining Medical University, Rizhao, Shandong, China*

Edited by Karin Musier-Forsyth

The potential antimicrobial compound Chuangxinmycin (CXM) targets the tryptophanyl-tRNA synthetase (TrpRS) of both Gram-negative and Gram-positive bacteria. However, the specific steric recognition mode and interaction mechanism between CXM and TrpRS is unclear. Here, we studied this interaction using recombinant GsTrpRS from *Geobacillus stearothermophilus* by X-ray crystallography and molecular dynamics (MD) simulations. The crystal structure of the recombinant GsTrpRS in complex with CXM was experimentally determined to a resolution at 2.06 Å. After analysis using a complex-structure probe, MD simulations, and site-directed mutation verification through isothermal titration calorimetry, the interaction between CXM and GsTrpRS was determined to involve the key residues M129, D132, I133, and V141 of GsTrpRS. We further evaluated binding affinities between GsTrpRS WT/mutants and CXM; GsTrpRS was found to bind CXM through hydrogen bonds with D132 and hydrophobic interactions between the lipophilic tricyclic ring of CXM and M129, I133, and V141 in the substrate-binding pockets. This study elucidates the precise interaction mechanism between CXM and its target GsTrpRS at the molecular level and provides a theoretical foundation and guidance for the screening and rational design of more effective CXM analogs against both Gram-negative and Gram-positive bacteria.

Antimicrobial resistance (AMR) is a global public health concern, for the misuse and overuse of antimicrobials in the past 50 years have caused and accelerated the development of drug-resistant pathogens (DRPs) (1). As AMR spreads worldwide, it is more and more difficult to treat infections and death caused by DRPs. Therefore, the urgent need has been provoked for exploring novel and more effective antimicrobials on the AMR issue. At molecular level, most antibiotics in clinical use nowadays mainly target the bio-macromolecules involved in the protein translation process, through interacting with microbial ribosomes and binding directly to rRNA or ribosomal subunit proteins. However, for drug targets, there are other macromolecular candidates beyond ribosomes within the broader scenario of protein translation process. One of such targets for existing and future antimicrobials is the aminoacyl-tRNA synthetase (aaRS) family. The aaRSs are ubiquitously expressed and play a critical role in the translation of genetic codes through synthesizing aminoacyl-tRNAs. Moreover, the aaRSs and tRNA are also important in the evolution of the universal genetic code and the shaping of codon assignments (2). Owing to the essential role of aaRS in maintaining the fidelity of translation, compounds that inhibit aaRSs are widely used in the treatment of infectious diseases or therapeutic applications against cancers and autoimmune (3–5). For instance, Mupirocin, an antibacterial drug targeting at isoleucyl tRNA synthetase of Gram-positive bacteria and having the required selectivity for prokaryotes over eukaryotes, is currently used, in clinic for the topical treatment of *Staphylococcus aureus* (6); Tavaborole (7), which targets fungal cytoplasmic leucyl-tRNA synthetase, is the first oxaborole antifungal agent approved by Food and Drug Administration in 2014. The structural and mechanistic differences among the different aaRS enzymes as well as orthologs of individual synthetases make it possible to selectively modulate their specific activity against different kinds of pathogens. This approach makes the aaRS enzymes attractive target candidates for developing novel anti-infective therapeutics.

Chuangxinmycin (CXM), a novel antibiotic containing an indole-dihydrothiopyran heterocyclic skeleton, was isolated from *Actinoplanes tsinanensis* CPCC 200056 (8). It exhibited *in vitro* antibacterial activity against both Gram-negative and Gram-positive bacteria, such as *Escherichia coli* and *S. aureus* (9), respectively, and showed no cross-resistance with common antibiotics, low toxicity, and few of side effects. Specifically, in a preliminary clinical trial, the CXM exhibited antibacterial effectiveness against septicemia, urinary, and biliary infections caused by *E. coli* (8). As at molecular level, CXM is an inhibitor of bacterial tryptophanyl-tRNA synthetase (TrpRS) (IC_{50} value of 30 nM against *S. aureus* TrpRS) (10). However, CXM's clinical use has been limited by its narrow spectrum of activity, the fact that it is only available in oral forms, and its relative

‡ These authors equally contributed to this work.
* For correspondence: Zhaoyong Yang, zhaoyongy@imb.pumc.edu.cn; Maocai Yan, yanmaocai@126.com.

lower antimicrobial activity in comparison with first-line antibiotics. Although CXM has not come into clinical use, its specific antibacterial mechanism through selectively inhibiting prokaryotic TrpRSs and its unusual heterocyclic skeleton with a sulfur have attracted the interests of pharmacologists and medicinal chemists. In addition, the biosynthesis studies of CXM had been previously reported by several groups (11, 12). A number of its analogs were also tested for their *in vitro* antibacterial activity (9, 10). Yet, regrettably, none of them showed higher antibacterial activity against *E. coli* or *S. aureus* than CXM. Nevertheless, if we could understand the structural basis and molecular mechanism of the TrpRS inhibition by CXM, we would be able to use structure–activity relationships in the rational design of CXM derivatives more effectively targeting at the TrpRSs of pathogens. So, a thorough understanding of the role of structure of TrpRS structure on their specificity and activity is essential in exploring CXM derivatives as antimicrobial drugs.

By far, the structural studies of TrpRSs from *Geobacillus stearothermophilus* (GsTrpRS) (13–16), *Saccharomyces cerevisiae* (ScTrpRS) (17), and *Homo sapiens* (hTrpRS) (18–21) have investigated the common recognition mode of aminoacyl-adenylate AMP and provided insights into the structural basis of the coupling of specificity and catalysis. Based on the architecture of the catalytic domains, aaRS are naturally divided into two classes (I and II). GsTrpRS is the smallest aaRS monomer and belongs with tyrosyl-tRNA synthase in subclass Ic, characterized by a central domain largely comprising of Rossmann dinucleotide-binding fold, which features the β/α/β Rossmann domains (residues M1–P198). Moreover, the helical domain consists of four α-helices (residues N199–Y260) and possesses three loops with exceptionally high mobility. The last 60 or so amino acids (residues S252–R326) form a long, discontinuous α-helix, running from one extremity to the dimer axis. Several previously structure-solved GsTrpRSs were each crystallized with different ligands: ATP (15), Tryptophan/AMP (22), tryptophanyl-5′AMP (13), and adenosine tetraphosphate (23). These structures provide the structural basis for substrate binding and catalytic mechanism. Arguably, GsTrpRS is one of the most extensively characterized TrpRS enzymes (24–27). Indolmycin is a natural tryptophan analog exhibiting high selectivity for bacterial TrpRS. The structural complex of GsTrpRS/indolmycin/ATP (28) was determined to elucidate the structural basis for the high affinity inhibition of GsTrpRS by indolmycin. In contrast to the pretransition state of TrpRS from *H. sapiens* (hTrpRS), different transition state stabilization mechanism results in a selectivity favorite toward bacterial TrpRSs by indolmycin. Interestingly, CXM was also highly selective for the bacterial TrpRS, with no inhibition on ovine TrpRS observed at concentrations up to 30 μM. Chuangxinmycin differs from indolmycin in the following ways: (i) although the two compounds share an indole substructure in their scaffold, CXM forms a tricyclic ring system which makes its conformation very rigid; (ii) Chuangxinmycin retains a free carboxylic acid group, whereas indolmycin forms an oxazolone and loses the carboxylic acid group; (iii) the lipophilic tricyclic scaffold of CXM facilitates its hydrophobic interactions with the binding pocket of its target. Overall, the structure of CXM is different from that of existing antibiotics, as it is connected to an indole fused onto a dihydrothiopyran ring (Fig. 1).

In this work, the determination of the GsTrpRS/CXM complex structure at a resolution of 2.06 Å allowed us to probe and report the key structural elements and residues for CXM recognition and molecular mechanism of inhibition. We also present the results of molecular dynamics (MD) simulation of the GsTrpRS/CXM structure and carried out functional analyses using isothermal titration calorimetry (ITC) on a series of mutants of the GsTrpRS. These analytic results not only reveal the structural motif crucial for the recognition and binding CXM, but also provide a structural basis and guidance for the rational design of CXM analogs of high antimicrobial potential for DRPs treatment.

Results and discussion

Overall structure of GsTrpRS/CXM complex

The TrpRS is a conserved and ubiquitously expressed protein in prokaryotes. Specifically, the protein sequence of GsTrpRS share 55%, 57%, and 52% identity with the TrpRS protein sequences from *Haemophilus influenzae*, *Yersinia pestis*, and *Vibrio cholerae*, respectively (Fig. S1). Therefore, it is convenient for us to probe the structural interaction mode for CXM inhibition by determining the structure of GsTrpRS/CXM binary complex on the basis of homologous structures. The crystal structure of GsTrpRS in complex with CXM was solved using molecular replacement method and the refinement of the final structure model converged to an R-factor of 0.1694 and a free R-factor of 0.2087 to 2.06 Å resolution. The binary complex crystal grew in the hexagonal $P3_221$ space group (a = b = 91.675 Å, c = 152.37 Å, α = β = 90°, γ = 120°). The crystallographic asymmetric unit of GsTrpRS/CXM crystal contains two subunits (subunit A and subunit B) (Fig. 2). As for the functional activity, the GsTrpRS would demonstrate three regular transition states: open state, closed pretransition state (PreTS), and closed products state (13–15). Presently, the structures of the GsTrpRS in different states have been reported, such as open Trp complex (PDB: 1MB2) (15), closed PreTS complex (PDB: 1M83) (15), closed PreTS tryptophanamide·ATP complex (PDB: 1MAU) (15), and closed product complex (PDB: 1I6L) (14). Structural differences between the CXM complex and those reported previously for the open and closed conformations are subtle. Superposition of the subunit A and the those said reported complexes on Cα atoms yields RMSD values of 0.620 Å (1MB2), 1.168 Å (1M83),

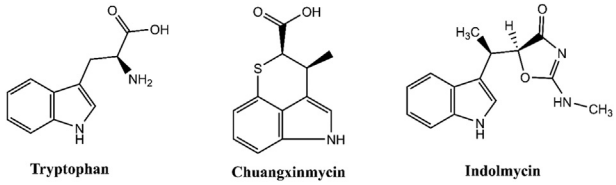

Figure 1. Functional equivalences of tryptophan, Chuangxinmycin, and Indolmycin.

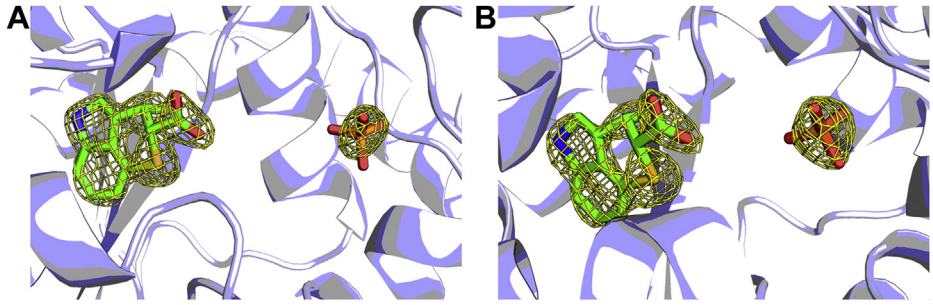

Figure 2. Electron-density map of CXM. *A*, the 2Fo–Fc map of CXM and phosphate group in subunit A; *B*, 2Fo–Fc map showing the CXM and phosphate group in subunit B. 2Fo–Fc map showing the CXM and phosphate group calculated at 2.0 σ. The CXM and phosphate group are modeled as *sticks* and colored as carbon (*green*), nitrogen (*blue*), oxygen (*red*), sulfur (*yellow*), and phosphorus (*orange*). CXM, Chuangxinmycin.

1.163 Å (1MAU), and 1.067 Å (1I6L), respectively, whereas the superposition of the subunit B and those reported complexes with corresponding Cα atoms gives out RMSD values 0.988 Å, 0.703 Å, 0.705 Å, and 0.886 Å, respectively. So, an interesting phenomenon emerges that GsTrpRS/CXM complex contains two distinct states, in which the subunit A is with open state and the subunit B is with closed PreTS state. The crystal structure of the CXM complex shows that GsTrpRS retains an open conformation and a closed PreTS conformation when bound simultaneously to CXM and inorganic phosphate. The position of phosphate ions in subunit A and B are found in coincidence with β-phosphate and α-phosphate in crystals containing ATP (1MAU), respectively (Fig. S2). The distance between the β/α-phosphate position and the phosphate ions bound to the GsTrpRS/CXM is 2.6 Å and 4.4 Å, respectively. To summarize, there are phosphate ions bound at the active site, which mimics an intermediate state of the β- or α-phosphate group of ATP. Unfortunately, because of the disorder at the loop P177-V179 of subunit B, the three amino acids (P177–V179) were not able to model into the final structure. As shown in Figure 3, the structure of GsTrpRS/CXM displays the conserved Rossmann dinucleotide-binding fold domain (residues M1–I14, H31–R182, and E294–R326) and small domain (residues T15–Q30 and I183–M293), as mentioned earlier (13). The final structure shows a good overall quality as evidenced by the statistics presented in Table 1.

Comparisons were carried out between the subunit A and subunit B in the asymmetric unit. Superimposing the subunit A to subunit B leaves RMSD 0.667 Å between corresponding Cα atoms, revealing the conformation of subunit A is similar to subunit B. However, the binding mode of CXM in subunit A is distinguished from that of subunit B. In contrast with subunit A, subunit B exhibits a more compact structure (Fig. 3*B*). To further investigate the differences in the conformation of the two subunits, we performed the following analyses.

Chuangxinmycin binding

Our crystal structure of the GsTrpRS in complex with CXM, provides the structurally binding details, at atomic level, of CXM inhibitory mechanism for the first time. For subunit A and B, the overall structures are quite similar; however, there are several differences on the hydrogen bonding and hydrophobic interactions between the CXM and amino acid residues of GsTrpRS. Specifically, the indyl group of CXM is within the hydrogen bonding distance of the carboxyl group of the side chain of D132 in the binary complex (Fig. 4). Meanwhile, the carboxyl of CXM in subunit A forms a hydrogen bond with amino acid residue Y125 (Fig. 4*A*). However, surprisingly, the carboxyl group of CXM forms a salt bridge with K195 in subunit B (Fig. 4*B*). The hydrophobic interactions also play critical roles in the binding of CXM. The structure of binary complex suggests that there could be the hydrophobic interactions between CXM and F5, V40, I133, V141, and V143 (Fig. 4). These critical amino acid residues except F5 have been considered conserved in comparison with homologous proteins.

In contrast to the reported GsTrpRS structure conformation, the subunit A of GsTrpRS/CXM structural complex shows in an open state and subunit B shows in a closed PreTS state. The CXM occupies the Trp-binding site and interacts with D132, Y125, or K195. Importantly, no significant changes of the conformation of the D132 are observed in the structure

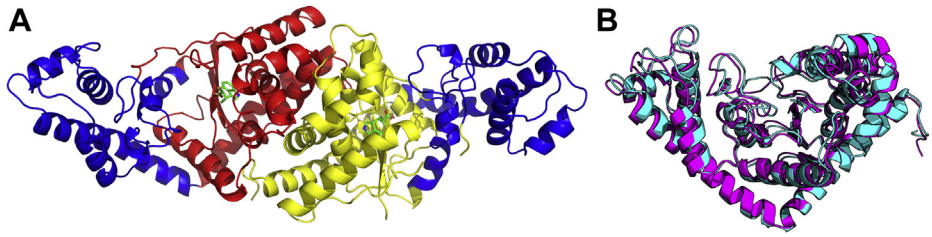

Figure 3. Crystallographical view of CXM bound to GsTrpRS. *A*, zoom-in view of CXM localization in GsTrpRS. Domain SD, RF-αA (subunit A), and RF-αA (subunit B) are drawn in *blue*, *red*, and *yellow*, respectively. Chuangxinmycin (*green*) are shown as a *stick* model; *B*, superimposition of subunit A to subunit B in the binary complex, with the former shown in *magenta* and the latter *cyan*, respectively. CXM, Chuangxinmycin; RF-αA, Rossmann dinucleotide-binding fold domain; SD, small domain; TrpRS, tryptophanyl-tRNA synthetase.

Table 1
Data collection and structure refinement statistics

Dataset	GsTrpRS/CXM
Data collection	
Space group	$P3_221$
Cell dimensions	
a, b, c (Å)	91.675, 91.675, 152.37
α, β, γ (°)	90.00, 90.00, 120.00
Resolution (Å)	50.00–2.06 (2.10–2.06)
$I/\sigma I$	23.23 (1.95)
Completeness (%)	100 (100)
Redundancy	18.6 (18.4)
Refinement	
Resolution (Å)	50.00–2.06(2.10–2.06)
Unique reflections	46,939 (2350)
Redundancy	18.6 (14)
R_{work}/R_{free}	0.1694/0.2087
Average B-factors	
Protein	26.35
Ligand/ion	28.05
R.m.s. deviations	
Bond lengths (Å)	0.007
Bond angles (°)	0.903
Ramachandran	
Favored (%)	96.17
Outliers (%)	0
Protein Data Bank Code	7CMS

Values in parentheses are for the highest resolution shell. R_{free} calculated with 5% of all reflections excluded from refinement stages using high resolution data.

of unliganded- (PDB: 1D2R), CXM- (PDB: 7CMS), Trp- (PDB: 1MB2), indolemycin- (PDB: 5DK4), and tryptophanamide-GsTrpRS (PDB: 1MAU) (Fig. 5). The carboxyl of CXM in subunit A forms a hydrogen bond with amino acid residue Y125. However, surprisingly, in subunit B, the carboxyl group of CXM forms a salt bridge with K195. In the structure of subunit B, the side chain of K195 adopts a distinct conformation from that in the unliganded GsTrpRS to accommodate binding of CXM (Fig. 5*A*). One observation is the loop containing $_{192}$KMSKS$_{196}$ of the CXM-bound GsTrpRS, which shows an inward movement toward the CXM-binding cavity when compared to the unliganded GsTrpRS (Fig. S3). In other words, binding of CXM to GsTrpRS induces a conformational transition of loop containing $_{192}$KMSKS$_{196}$ from an open state to a closed PreTS state.

Molecular dynamics simulations for interaction analysis and evaluation of binding free energy

The prediction of antibiotic activity by MD simulation would be highly valuable for the antibiotic discovery. Molecular dynamics simulation are reliable methods to explore protein–ligand interactions at the atomic and molecular levels. It can provide a deeper understanding of the intermolecular energy contributions. In this study, MD simulations were performed to predict the resistance for the CXM and to gain further insight into the contributions of the binding free energy of different GsTrpRS mutants. During MD simulation, the trajectory reached a relatively stable status when the RMSD and energy kept steady at 12 ns (Fig. S4*A*). After RMSD convergence of the MD trajectory, binding mode of CXM to TrpRS was analyzed. The initial structure and the structure at 20 ns were aligned with their protein Cα atoms (RMSD = 1.91 Å) and shown in Fig. S4*B*. It is obvious that the protein scaffold kept steady and did not change significantly in the MD simulations; the ligand-binding poses were similar before and after MD simulations, despite of a slight translation (Fig. S5). The receptor–ligand interaction mode was displayed in Figure 5. Owing to the hydrophobic scaffold of CXM, it mainly formed hydrophobic interactions with TrpRS, including M129, Q147, V143, G7, V40, I133, etc. The indole nitrogen atom formed a hydrogen bond with D132 carboxylate anion. The carboxylate anion of CXM pointed to the ATP pocket and did not form any interactions with GsTrpRS residues.

The average Generalized Born Surface Area (GBSA) binding free energy of CXM to TrpRS of 12∼20 ns period was calculated to be −17.3 kcal/mol (note that the binding entropy, which is usually a negative value, was ignored in the calculation, so the actual binding free energy is likely higher than this value). To further evaluate the contribution of each amino acid residue to the ligand binding, contribution of amino acid residues around the CXM-binding site were analyzed by decomposing the binding free energy to each residue sidechain and by virtually mutating each residue to alanine in the GBSA calculation

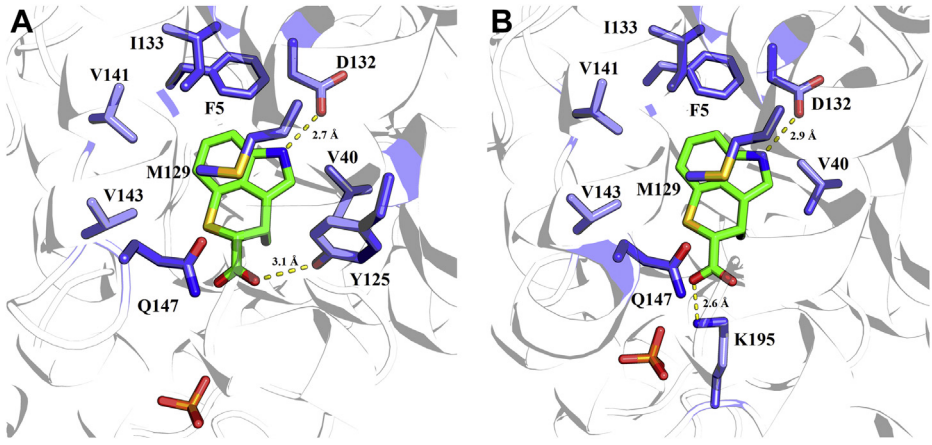

Figure 4. Schematic representation of the hydrogen-bond and hydrophobic interaction between CXM/ATP and GsTrpRS. Diagrams *A* and *B* show hydrogen-bond interactions of CXM at substrate-binding sites of subunit A and subunit B, respectively. Chuangxinmycin (*green*) and crucial amino acid residues of GsTrpRS (*blue*) are shown as *sticks* and *labeled*. The *dashed lines* indicate hydrogen-bond (*yellow*) interactions. CXM, Chuangxinmycin; TrpRS, tryptophanyl-tRNA synthetase.

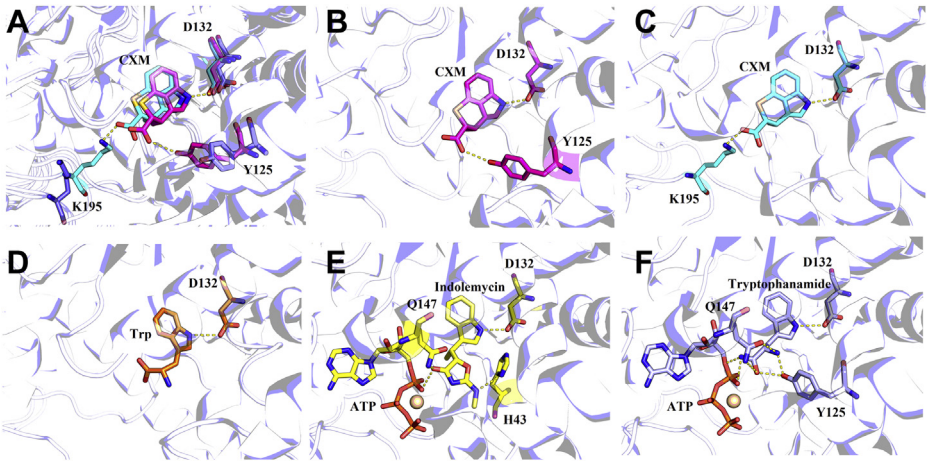

Figure 5. Substrate-binding mode of GsTrpRS structural complexes. *A*, comparison of the substrate-binding sites of ligand-free and CXM-bound GsTrpRS; *B* and *C*, subunit A and subunit B of CXM-bound GsTrpRS; *D*, trp-bound GsTrpRS; *E*, indolemycin/ATP/Mg^{2+}-bound GsTrpRS; *F*, tryptophanamide/ATP/Mg^{2+}-bound GsTrpRS. Ligand-free, subunit A, subunit B, trp-bound, indolemycin/ATP/Mg^{2+}-bound, and tryptophanamide/ATP/Mg^{2+}-bound of GsTrpRS are shown in *blue*, *magenta*, *cyan*, *orange*, *yellow*, and *light blue*, respectively. Mg^{2+} (wheat) are shown as *sphere* model. The *dashed lines* indicate hydrogen-bond (*yellow*) interactions. CXM, Chuangxinmycin; TrpRS, tryptophanyl-tRNA synthetase.

(Table 2). This evaluation was also accomplished in AmberTools 18. It is clear that lipophilic residues including Q147, M129, V40, and I133 played very important roles in ligand binding, followed by V141, F5, V143, H43, etc. Interestingly, most of the amino acid residues (V40, M129, D132, I133, V141, V143, and Q147) were considerably conserved among the members of pathogenic bacteria. The polar residues S6, E110, and D146 showed little or negative contributions to the ligand binding. The evaluation results of free energy decomposition and alanine scanning agreed with each other roughly; however, D132, which formed an important hydrogen bond with CXM and exhibited an outstanding contribution to ligand binding in alanine scanning, displayed a negative contribution (+1.21 kcal/mol) in free energy decomposition analysis.

Charting the thermodynamic parameters of the GsTrpRS and mutants via *ITC*

It is generally accepted that the amino acids that participate in the substrate binding or catalytic sites are crucial for the catalysis or inhibition. The following amino acid residues of GsTrpRS, F5, I8, V40, H43, Q80, Y125, M129, D132, I133, V141, and Q147, are selected as "hot spots" to identify putative residues participating in the binding of CXM. Isothermal titration calorimetry was used to evaluate the thermodynamic parameters of GsTrpRS and mutants. We used ITC and L-alanine scanning mutagenesis to further characterize the interaction between the WT/mutants with CXM (Fig. S6). The interaction of CXM with GsTrpRS was found to be connected with a negative ΔH, so the interaction is driven by enthalpy consistent with the results of the conserved hydrogen bond formed by D132 playing a significant role in substrate binding. The results (Table 3) showed that M129A, D132A, I133A, and V141A mutants had no measurable binding affinity against CXM, which was consistent with the function of these residues as binding site residues. Similarly, the binding affinity parameters showed that the K_d value of the V40A and Q80A mutations were 10.4/14.8 times more than that of the WT, respectively. That is to say, V40A and Q80A exhibited decreased binding affinity against CXM compared with the WT. The results show that the binding affinity of K195A for CXM is not changed. Concretely, the hydrogen bond is broken by mutation of Lys195 to hydrophobic amino acid (alanine). This led to the conclusion that the mutant K195A have decreased enthalpy and increased entropy in the binding CXM. The CXM affinity we observed with H43A (5.5 μM) and Y125A (2.1 μM), although largely consistent with that of WT (3.1 μM), decrease in the enthalpy change ΔH. In addition, in the case of F5A and K195A, the contribution of entropy to the overall free energy change of interaction is larger than that of WT. The −TΔS of WT are 3.5 kcal/mol, whereas those of F5A and K195A are −1.6 kcal/mol and −1.3 kcal/mol, respectively. Unexpectedly, there was no significant change in the affinity of CXM for Q147A used as "hot spots" in GBSA calculation. Further studies need to be performed to investigate this in more details.

Table 2
Contribution of sidechain of key residues to the binding-free energy (kcal/mol), evaluated by free energy decomposition and virtual alanine scanning

Residue	Free energy decomposition	Alanine scanning
Q147	−1.12	−1.95
M129	−1.34	−1.55
V40	−0.81	−1.29
I133	−0.73	−1.26
D132	1.21	−0.83
V141	−0.46	−0.76
F5	−0.25	−0.75
V143	−0.45	−0.65
H43	−0.01	−0.63
K111	−0.20	−0.35
Q80	−0.09	−0.34
I8	−0.43	−0.32
Y125	−0.03	−0.01
G7	−0.32	N/A
Q9	−0.17	0.05
D146	0.13	0.16
E110	0.09	0.18
S6	−0.23	0.21

Structural basis for CXM inhibition

The structural and computational study on the interaction of inhibitor with its target is essential in drug discovery and

Table 3
Determination of affinity between GsTrpRS WT/mutants and CXM

Mutant	K_d (μM)	N	ΔH (kcal/mol)	Δ*G* (kcal/mol)	−TΔ*S* (kcal/mol)
WT	3.1 ± 0.1	0.8	−11.1 ± 0.3	−7.6	3.5
WT·Mg^{2+}-ATP	4.3 ± 1.0	0.8	−10.4 ± 2.1	−7.3	3.1
F5A	3.3 ± 0.2	0.7	−5.9 ± 0.3	−7.5	−1.6
I8A	16.2 ± 1.1	0.7	−7.8 ± 0.7	−6.5	1.3
V40A	32.1 ± 1.2	0.8	−8.0 ± 0.4	−6.1	1.9
H43A	5.5 ± 0.8	0.6	−19.8 ± 0.9	−7.2	12.6
Q80A	47.5 ± 3.8	0.8	−8.0 ± 0.5	−5.9	2.1
Y125A	2.1 ± 0.1	0.7	−14.2 ± 1.3	−7.7	6.5
M129A	NA	NA	NA	NA	NA
D132A	NA	NA	NA	NA	NA
I133A	NA	NA	NA	NA	NA
V141A	NA	NA	NA	NA	NA
Q147A	9.4 ± 0.2	0.7	−8.3 ± 0.1	−6.9	1.46
K195A	1.4 ± 0.3	0.6	−6.7 ± 0.7	−8.0	−1.3

development. To validate what factors account for the observed binding affinity of CXM, we analyzed the binding free energy by GBSA calculation and then conducted ITC experiment in the presence of various mutants. The structure of binary complex and binding free energy calculation clearly showed novel aspects of CXM inhibitory action. Specifically, the binding of CXM to the GsTrpRS, calculated from the ITC binding data, was found to be enthalpy driven. Thus, we identified and analyzed the structure of binary complex and found that the configuration of the hydrogen-bonding network varies the structure, but the hydrogen bond formed between CXM and D132 is predominant in the binary complex. The interaction between Oδ2 of D132 in the specificity helix and the nitrogen atom of the indole ring is observed when tryptophan (22), tryptophanamide (14), or indolmycin (28) is bound. Meanwhile, mutation of aspartic acid to alanine (D132A) indeed abolished the binding affinity of GsTrpRS as shown in our ITC experiment (Table 3). To further verify the crucial residues in ligand binding, the binding free energy of CXM was calculated by using a modified molecular mechanics (MM)/GBSA method. The combined results of energy decomposition and alanine scanning showed that lipophilic residues including Q147, M129, V40, and I133, played crucial roles in ligand binding, followed by V141, F5, V143, H43, etc. These residues were tested by site-directed mutagenesis and ITC measurement experiments. The data of ITC allowed us to further analyze the role of the individual thermodynamic parameters in the mechanism of binding CXM associated with the mutations. According to the results of the ITC experiments, it is interesting to note that mutants M129A, I133A, and V141A are unable to bind CXM. By contrast, the single amino acid mutation V40A and Q80A had negatively impacts on the binding affinity compared to the WT. In summary, these residues, M129, D132, I133, and V141, were considered the key residues to stabilizing and orienting the substrates for the binding.

Here, we have elucidated the interactions of GsTrpRS with the indole-dihydrothiopyran heterocyclic molecule CXM, which may function as a prospective new antibacterial agent for treating the regular bacterial, even DPRs, infections. The thiopyran ring of CXM, stabilized by hydrogen bonds with D132 and Y125 or K195, prevents the rotamer switch of Y125 in the specificity helix when in molecular interaction; this rotamer switch is part of the structural transition from the open to the closed state, and this opening results in a weakening outcome of ATP–GsTrpRS interactions, specifically those between K111 and the γ-phosphate group. As an effort to improve the antimicrobial activity of CXM and to optimize its physicochemical parameters, here, we present some suggestions which may be useful for medicinal chemists in future for the structural optimization of CXM. Mutation of M129, D132, I133, and V141 residues leads to loss of the high affinity of CXM. Obviously, the indole ring plays a critical role on the binding affinity of CXM (Fig. 5*A*). Therefore, no modifications, to a great extent, of indole ring are recommended. Nevertheless, GsTrpRS has a relatively big substrate-binding cavity, indicating that the sulfur atom of thiopyran could be associated with a small hydrophobic group that could occupy the extra hydrophobic cavity of CXM pocket, to increase the binding affinity. The methyl of CXM could be replaced by larger moieties, such as ethyl, because the CXM-binding pocket has sufficient space. In this case, the CXM derivative may form additional hydrophobic interactions with amino acid residues in the CXM-binding pocket. The carboxyl group could be modified by polar groups, such as sulfonic acid, amide, and sulfonamide, in further structural modifications, to find novel ligands with higher-binding affinity and structural diversity (Fig. 6*B*).

Conclusions

In summary, our structural and functional studies of GsTrpRS/CXM provide a framework to elucidate the molecular basis of binding and inhibitory mechanism of CXM to GsTrpRS. The determined GsTrpRS crystal structure in complex with CXM is expected to serve as a guidance for the design and optimization of molecular structures of CXM and analogs to develop novel drug candidates against Gram-negative and Gram-positive bacteria.

Experimental procedures

Cloning and site-directed mutagenesis of GsTrpRS

The gene encoding the GsTrpRS was codon-optimized and synthesized by Beijing Genomics Institute. It was PCR-

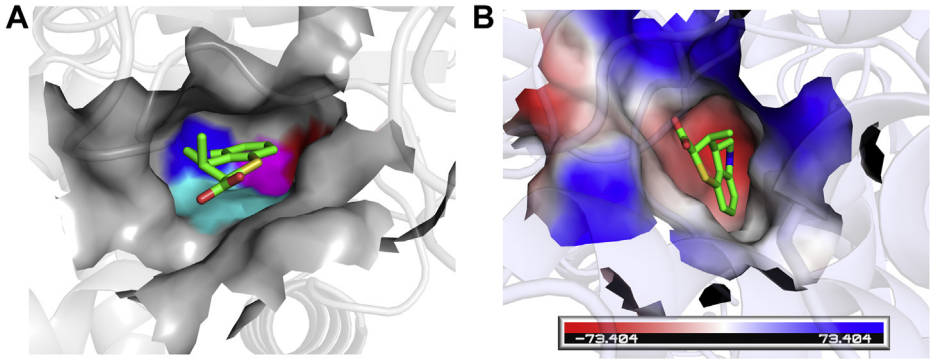

Figure 6. Binding mode of CXM to TrpRS after 20-ns MD simulations. *A*, a view of the CXM binding onto GsTrpRS. Highlighted in surface view are the amino acids involved in shaping the substrate pocket. M129 (*cyan*), D132 (*blue*), I133 (*magenta*), and V141 (*red*) are shown as surface; *B*, receptor surface was colored with hydrophobicity. Chuangxinmycin (*green*) are shown as *stick* model. CXM, Chuangxinmycin; TrpRS, tryptophanyl-tRNA synthetase.

amplified by KOD FX Neo DNA Polymerase (TOYOBO) with a set of primers GsTrpRS-F:5′-GGAATTCCATATGGGTAT GAAAACCATTTTTAGCG-3′ and GsTrpRS-R: 5′- CCGCTC GAGGCGGCGACGACCCAGACCCATA-3′, which contained an N-terminal *Nde*I and a C-terminal *Xho*I restriction site (underlined), respectively. The *GsTrpRS* gene was cloned into the expression vector pET-21a (+) (Novagen) by virtue of the *Nde*I and *Xho*I restriction sites, for the production of recombinant GsTrpRS protein extended at the C-terminus by a six-histidine tag. Site-directed mutagenesis of the amino acids with the *GsTrpRS* gene was achieved by overlapping extension PCR to make recombined pET21a-mutant plasmids. After the verification of the sequences, these plasmids containing modified-*GsTrpRS* genes were transformed respectively into the competent BL21 (DE3) for heterologous expression. All cloned expression constructs were checked for accuracy by DNA sequencing. All oligonucleotide primers are listed in Table S1.

Enzyme production and purification

Both GsTrpRS and mutants were overexpressed in *E. coli* strain BL21(DE3) supplemented with 0.5 mM isopropyl-β-D-1-thiogalactopyranoside at an absorbance of 0.6 at 600 nm (A_{600}) followed by a reduction of growth incubation temperature from 37 °C to 18 °C for 12 h. The cells were harvested by centrifugation at 6000*g* for 15 min at 4 °C and resuspended in 20 ml lysis buffer (20 mM phosphate buffer, 300 mM NaCl, 10 mM imidazole, pH 7.4) containing 1 mM PMSF. The cells were disrupted by high pressure homogenizer and the soluble fraction was separated by centrifugation (60,000*g* at 4 °C for 40 min) and passed through a 0.45 mm filter, and the cleared supernatant was immediately applied to 2 ml TALON Metal Affinity Resin (Clotech) loaded on a column which was pre-equilibrated with lysis buffer. The resin was subsequently washed with 10 ml washing buffer (20 mM phosphate buffer, 300 mM NaCl, 20 mM imidazole, pH 7.4). Elution was carried out with 10 ml elution buffer (20 mM phosphate buffer, 50 mM NaCl, 250 mM imidazole, pH 7.4). Fractions containing GsTrpRS were pooled and further purified by Superose 12 10/300 GL (GE Healthcare) in 50 mM Tris pH 7.2, 100 mM PMSF at a flow rate of 0.5 ml/min. Purity was ascertained by SDS–PAGE, and the target protein has a molecular weight of about 38 kDa, in agreement with the expected GsTrpRS size. The final protein was flash-frozen in liquid nitrogen and stored at −80 °C.

Crystallization, X-ray diffraction, and data collection

The initial crystallization screening was performed with Crystal Screen HR2-110 and HR2-112 (Hampton Research) as well as Wizard CRYO I and Wizard CRYO II (Rigaku), by using hanging drop vapor diffusion method at 37 °C, then, the positive hits were optimized. After optimizing the conditions, the crystals of the GsTrpRS/CXM were obtained from drops with the crystallization solution containing 1.8 M K_2HPO_4, pH 7.6, 1,3-Propanediol (1.5% v/v). The X-ray diffraction data were collected at BL18U1 at Shanghai Synchrotron Radiation Facility, using a CCD detector with beam at wavelength 0.97915 Å, and the data were processed and scaled by using HKL3000 (29).

Structure determination and refinement

The GsTrpRS/CXM complex structure was determined by using Molecular Replacement method. The program Phenix (30) was used to find an initial molecular replacement solution with a model based on the structure of GsTrpRS (PDB accession code 1I6M). After the *apo*-form structure was built, the shape of electron density within the substrate-binding pocket is consistent with the structural outline of CXM, and the molecule was fitted into the electron density. The structure was refined using data to 2.06 Å resolution. The high-resolution data allowed the structure refinement with Phenix (30), with additional rounds of manual model rebuilding in Coot (31), until the R_{work} and R_{free} values got to 0.1694 and 0.2087, respectively. The crystallographic and structural data statistics are listed in Table 1. The refined structure has been deposited in the Protein Data Bank with accession code 7CMS. Structural figures were drawn using the PyMOL software (http://www.pymol.org).

Molecular dynamics simulations

Preparation of the system

The cocrystal structure of TrpRS complexed with CXM (PDB entry: 7CMS) was used as initial structure of MD

simulations. All MD simulations were performed with Amber 18 (32). The net charge of CXM was set to −1 (carboxylate anion), and the partial charges were calculated with Antechamber module in AmberTools 18. The GAFF force field parameters of CXM were generated with parmchk2 and tleap module in AmberTools 18. Amber ff14SB force field was applied to the protein, and TIP3P model was used for the water molecules. A truncated octahedron solvent box was added to dissolve the protein, and sodium cations were added to neutralize the system. The final system contains 13,524 water molecules and seven Na^+ ions.

Molecular dynamics simulations

For energy minimizations, firstly, all atoms in the protein and CXM were restrained, and the system was minimized for 2000 steps; then restraints on the ligand were removed and the system was further minimized for 5000 steps; finally, all the restraints were removed and another 10,000 steps minimization were performed. In the equilibration phase, the protein was restrained and NVT ensemble was used to heat the system to 300 K in 50 ps; then all the restraints were removed and the system was equilibrated with NPT ensemble for 1 ns. In the production phase, the system was simulated for 20 ns at 300 K (NPT ensemble).

Binding free energy calculation and decomposition

The MM/GBSA method, which has been implemented in AmberTools 18, was used to evaluate the binding free energy of CXM to TrpRS. The binding entropy was ignored, because the reliability of entropy calculation in GBSA or PBSA method is relatively low. The 20-ns trajectory in the production phase was analyzed, and the trajectory after RMSD convergence (12∼20 ns) was selected for the binding free energy calculation and decomposition (using MM/PBSA module in AmberTools 18).

Isothermal titration calorimetry

The ITC experiments were conducted with a MicroCal PEAQ-ITC system (Malvern Instruments) Microcalorimeter. This device was connected to a computer with MicroCal PEAQ-ITC software to control the device and record data. Before every experiment, 280 μl of 30 μM GsTrpRS solution was loaded to the sample cell, and 150 μM of CXM solution was loaded to the injection syringe. After the equilibration time of the calorimeter, there was a 60 s delay before titration. The stirring speed was set to 800 rpm. The experiments were performed at least in duplicate using the following parameters: temperature, 25 °C; reference power, 5 μcal/s; injection volume, 0.2 μl first injection followed by 2 μl for the remaining 19 injections; spacing between injections, 200 s. The data were analyzed by Origin 7 software provided by the manufacturer with curves fitted with a one set of site models.

Data availability

Atomic coordinates and structure factors for the reported GsTrpRS/CXM structure have been deposited in the Protein Data Bank with PDB ID: 7CMS. All remaining data is presented in the main article and supporting information.

Supporting information—This article contains supporting information.

Acknowledgments—This work was funded by the National Key Research and Development Program of China (No. 2018YFA0901800), National Natural Science Foundation of China (Grants 81761128016 and 8187131584), CAMS Innovation Fund for Medical Sciences (2019-I2M-1-005), and NSFC cultivation project of Jining Medical University (JYP2018KJ18). We thank Prof. Zhuorong Li (Institute of Medicinal Biotechnology, Chinese Academy of Medical Sciences & Peking Union Medical College, China) for providing the Chuangxinmycin. We thank BL18U1 in Shanghai Synchrotron Radiation Facility (SSRF) for providing technical support and assistance in data collection and process. We also thank Mr Yi Han at the Institute of Biophysics Core-Facility for the support during in-house data collection.

Author contributions—S. F. and Z. Y. conceptualization; S. F. methodology; S. F. and G. L. investigation; S. F. writing–original draft; S. F. and Z. Y. funding acquisition; X. F. validation; G. W., Y. J., and M. Y. writing–review and editing; Z. Y. supervision; Z. Y. resources.

Conflict of interest—The authors declare that they have no conflicts of interest with the contents of this article.

Abbreviations—The abbreviations used are: aaRS, aminoacyl-tRNA synthetase; AMR, Antimicrobial resistance; CXM, Chuangxinmycin; DRPs, drug-resistant pathogens; GBSA, Generalized Born Surface Area; ITC, isothermal titration calorimetry; MM, molecular mechanics; PreTS, pretransition state; TrpRS, tryptophanyl-tRNA synthetase.

References

1. Holmes, A. H., Moore, L. S., Sundsfjord, A., Steinbakk, M., Regmi, S., Karkey, A., Guerin, P. J., and Piddock, L. J. (2016) Understanding the mechanisms and drivers of antimicrobial resistance. *Lancet* **387**, 176–187
2. Carter, C. W., Jr., and Wills, P. R. (2021) The roots of genetic coding in aminoacyl-tRNA synthetase duality. *Annu. Rev. Biochem.* **90**, 349–373
3. Kim, D. G., Lee, J. Y., Kwon, N. H., Fang, P., Zhang, Q., Wang, J., Young, N. L., Guo, M., Cho, H. Y., Mushtaq, A. U., Jeon, Y. H., Choi, J. W., Han, J. M., Kang, H. W., Joo, J. E., *et al.* (2014) Chemical inhibition of prometastatic lysyl-tRNA synthetase-laminin receptor interaction. *Nat. Chem. Biol.* **10**, 29–34
4. Rock, F. L., Mao, W., Yaremchuk, A., Tukalo, M., Crepin, T., Zhou, H., Zhang, Y. K., Hernandez, V., Akama, T., Baker, S. J., Plattner, J. J., Shapiro, L., Martinis, S. A., Benkovic, S. J., Cusack, S., *et al.* (2007) An antifungal agent inhibits an aminoacyl-tRNA synthetase by trapping tRNA in the editing site. *Science* **316**, 1759–1761
5. Zhou, H., Sun, L., Yang, X. L., and Schimmel, P. (2013) ATP-directed capture of bioactive herbal-based medicine on human tRNA synthetase. *Nature* **494**, 121–124
6. Nakama, T., Nureki, O., and Yokoyama, S. (2001) Structural basis for the recognition of isoleucyl-adenylate and an antibiotic, mupirocin, by isoleucyl-tRNA synthetase. *J. Biol. Chem.* **276**, 47387–47393
7. Elewski, B. E., Aly, R., Baldwin, S. L., Gonzalez Soto, R. F., Rich, P., Weisfeld, M., Wiltz, H., Zane, L. T., and Pollak, R. (2015) Efficacy and safety of tavaborole topical solution, 5%, a novel boron-based antifungal

agent, for the treatment of toenail onychomycosis: Results from 2 randomized phase-III studies. *J. Am. Acad. Dermatol.* **73**, 62–69
8. Studies on a new antibiotic–Chuangxinmycin. *Sci. Sin.* **20**, (1977), 106–112
9. Sun, L., Zhang, S., Hu, X., Jin, J., and Li, Z. (2019) Synthesis, resolution, derivatization and antibacterial activity of Chuangxinmycin. *Future Med. Chem.* **11**, 2877–2890
10. Brown, M. J., Carter, P. S., Fenwick, A. S., Fosberry, A. P., Hamprecht, D. W., Hibbs, M. J., Jarvest, R. L., Mensah, L., Milner, P. H., O'Hanlon, P. J., Pope, A. J., Richardson, C. M., West, A., and Witty, D. R. (2002) The antimicrobial natural product Chuangxinmycin and some synthetic analogues are potent and selective inhibitors of bacterial tryptophanyl tRNA synthetase. *Bioorg. Med. Chem. Lett.* **12**, 3171–3174
11. Shi, Y., Jiang, Z., Li, X., Zuo, L., Lei, X., Yu, L., Wu, L., Jiang, J., and Hong, B. (2018) Biosynthesis of antibiotic Chuangxinmycin from Actinoplanes tsinanensis. *Acta Pharm. Sin. B* **8**, 283–294
12. Xu, X., Zhou, H., Liu, Y., Liu, X., Fu, J., Li, A., Li, Y. Z., Shen, Y., Bian, X., and Zhang, Y. (2018) Heterologous expression guides identification of the biosynthetic gene cluster of Chuangxinmycin, an indole alkaloid antibiotic. *J. Nat. Prod.* **81**, 1060–1064
13. Ilyin, V. A., Temple, B., Hu, M., Li, G., Yin, Y., Vachette, P., and Carter, C. W., Jr. (2000) 2.9 A crystal structure of ligand-free tryptophanyl-tRNA synthetase: Domain movements fragment the adenine nucleotide binding site. *Protein Sci.* **9**, 218–231
14. Retailleau, P., Yin, Y., Hu, M., Roach, J., Bricogne, G., Vonrhein, C., Roversi, P., Blanc, E., Sweet, R. M., and Carter, C. W., Jr. (2001) High-resolution experimental phases for tryptophanyl-tRNA synthetase (TrpRS) complexed with tryptophanyl-5'AMP. *Acta Crystallogr. D Biol. Crystallogr.* **57**, 1595–1608
15. Retailleau, P., Huang, X., Yin, Y., Hu, M., Weinreb, V., Vachette, P., Vonrhein, C., Bricogne, G., Roversi, P., Ilyin, V., and Carter, C. W., Jr. (2003) Interconversion of ATP binding and conformational free energies by tryptophanyl-tRNA synthetase: Structures of ATP bound to open and closed, pre-transition-state conformations. *J. Mol. Biol.* **325**, 39–63
16. Doublie, S., Bricogne, G., Gilmore, C., and Carter, C. W., Jr. (1995) Tryptophanyl-tRNA synthetase crystal structure reveals an unexpected homology to tyrosyl-tRNA synthetase. *Structure* **3**, 17–31
17. Zhou, M., Dong, X., Shen, N., Zhong, C., and Ding, J. (2010) Crystal structures of Saccharomyces cerevisiae tryptophanyl-tRNA synthetase: New insights into the mechanism of tryptophan activation and implications for anti-fungal drug design. *Nucleic Acids Res.* **38**, 3399–3413
18. Shen, N., Zhou, M., Yang, B., Yu, Y., Dong, X., and Ding, J. (2008) Catalytic mechanism of the tryptophan activation reaction revealed by crystal structures of human tryptophanyl-tRNA synthetase in different enzymatic states. *Nucleic Acids Res.* **36**, 1288–1299
19. Yang, X. L., Guo, M., Kapoor, M., Ewalt, K. L., Otero, F. J., Skene, R. J., McRee, D. E., and Schimmel, P. (2007) Functional and crystal structure analysis of active site adaptations of a potent anti-angiogenic human tRNA synthetase. *Structure* **15**, 793–805
20. Kise, Y., Lee, S. W., Park, S. G., Fukai, S., Sengoku, T., Ishii, R., Yokoyama, S., Kim, S., and Nureki, O. (2004) A short peptide insertion crucial for angiostatic activity of human tryptophanyl-tRNA synthetase. *Nat. Struct. Mol. Biol.* **11**, 149–156
21. Shen, N., Guo, L., Yang, B., Jin, Y., and Ding, J. (2006) Structure of human tryptophanyl-tRNA synthetase in complex with tRNATrp reveals the molecular basis of tRNA recognition and specificity. *Nucleic Acids Res.* **34**, 3246–3258
22. Laowanapiban, P., Kapustina, M., Vonrhein, C., Delarue, M., Koehl, P., and Carter, C. W., Jr. (2009) Independent saturation of three TrpRS subsites generates a partially assembled state similar to those observed in molecular simulations. *Proc. Natl. Acad. Sci. U. S. A.* **106**, 1790–1795
23. Retailleau, P., Weinreb, V., Hu, M., and Carter, C. W., Jr. (2007) Crystal structure of tryptophanyl-tRNA synthetase complexed with adenosine-5' tetraphosphate: Evidence for distributed use of catalytic binding energy in amino acid activation by class I aminoacyl-tRNA synthetases. *J. Mol. Biol.* **369**, 108–128
24. Carter, C. W., Jr. (2020) Escapement mechanisms: Efficient free energy transduction by reciprocally-coupled gating. *Proteins* **88**, 710–717
25. Carter, C. W., Jr., Chandrasekaran, S. N., Weinreb, V., Li, L., and Williams, T. (2017) Combining multi-mutant and modular thermodynamic cycles to measure energetic coupling networks in enzyme catalysis. *Struct. Dyn.* **4**, 032101
26. Carter, C. W., Jr. (2017) High-dimensional mutant and modular thermodynamic cycles, molecular switching, and free energy transduction. *Annu. Rev. Biophys.* **46**, 433–453
27. Chandrasekaran, S. N., and Carter, C. W., Jr. (2017) Augmenting the anisotropic network model with torsional potentials improves PATH performance, enabling detailed comparison with experimental rate data. *Struct. Dyn.* **4**, 032103
28. Williams, T. L., Yin, Y. W., and Carter, C. W., Jr. (2016) Selective inhibition of bacterial tryptophanyl-tRNA synthetases by indolmycin is mechanism-based. *J. Biol. Chem.* **291**, 255–265
29. Minor, W., Cymborowski, M., Otwinowski, Z., and Chruszcz, M. (2006) HKL-3000: The integration of data reduction and structure solution–from diffraction images to an initial model in minutes. *Acta Crystallogr. D Biol. Crystallogr.* **62**, 859–866
30. Adams, P. D., Afonine, P. V., Bunkoczi, G., Chen, V. B., Davis, I. W., Echols, N., Headd, J. J., Hung, L. W., Kapral, G. J., Grosse-Kunstleve, R. W., McCoy, A. J., Moriarty, N. W., Oeffner, R., Read, R. J., Richardson, D. C., *et al.* (2010) PHENIX: A comprehensive Python-based system for macromolecular structure solution. *Acta Crystallogr. D Biol. Crystallogr.* **66**, 213–221
31. Emsley, P., and Cowtan, K. (2004) Coot: Model-building tools for molecular graphics. *Acta Crystallogr. D Biol. Crystallogr.* **60**, 2126–2132
32. Case, D. A., Belfon, K., Ben-Shalom, I. Y., Brozell, S. R., Cerutti, D. S., Cheatham, T. E., III, Cruzeiro, V. W. D., Darden, T. A., Duke, R. E., Giambasu, G., Gilson, M. K., Gohlke, H., Goetz, A. W., Harris, R., Izadi, S., *et al.* (2018) *AMBER 2018*, University of California, San Francisco